

PREDICTION OF THERMAL CONDITION OF CAGE-ROTOR INDUCTION MOTORS UNDER NON-STANDARD SUPPLY SYSTEMS

S.C.Mukhopadhyay
School of Engineering and Advanced Technology
Massey University
Palmerston North
New Zealand

Tel: 64 6 3505799, fax: 64 6 350 2259, Email: S.C.Mukhopadhyay@massey.ac.nz

Abstract-- A hybrid thermal model for accurate estimation of thermal condition of cage-rotor induction motors under non-standard supply systems has been presented. The developed thermal model is a combination of lumped and distributed thermal parameters which are available from motor dimensions and other physical constants. The thermal condition of the motor under non-standard supply systems such as unbalanced power supply, distorted power supply can be estimated and the necessary derating of the motor can be carried out. The simulated and experimental results are presented.

Index terms -- Thermal model, hybrid, cage-rotor, induction motor, distortion, harmonics, unbalanced supply, transient, derating.

I. INTRODUCTION

The motor designers usually design a motor on the assumptions that the motor will operate satisfactorily under a virtually sinusoidal and balanced supply system. But in practical situation, the input conditions to which the motor is subjected are seldom the same for which the motor was designed, rather the motors operate under non-standard supply systems. The common forms of non-standard power supply which are observed are: (i) voltage level variations from the nominal value, (ii) frequency variation, (iii) voltage unbalances between phases, and (iv) distortion in supply. The harmonics are introduced by the use of rectifiers, thyristors, magnetic circuit saturation of transformers and reactors etc. So the actual performance of the motor cannot be expected due to higher temperature rise, reduced torque, poor power factor etc. A good knowledge of internal thermal condition of the motor is very important for proper utilization of the motor, for optimum derating of the motor and to save the motor from burn-out [1, 2, 3, 4].

Since induction motors consume almost 85% of total energy consumption in the world it is very important to predict thermal condition of the motor and development of thermal model of motors started from early days. Combined electromagnetic-thermal model and lumped parameter aided approach have been used by many researchers which can provide the temperature of the motor under steady state operation [5-12].

Sometimes, the knowledge of transient thermal state is very important. In recent times different new techniques, implicit collocation technique with non-classic initial condition for solving the heat equation [13], direct solution of 2D heat transfer problem with non-linear source terms in

frequency domain [14], electromagnetic heating effects to stop crack propagation in metal components [15], temperature field around crack tip in a current-carrying plate under the repeated action of pulse current [16], a novel approach to the solution of temperature distribution on the stator of an induction motor [17] are reported.

This paper reports a hybrid thermal model which is a combination of lumped and distributed parameters and is suitable for the prediction of temperature profile of induction motors operating under non-standard supply systems, such as unbalanced power supply, distorted power supply as well the operation under nominal operating conditions. The complete paper has been divided into five sections. After the introduction in section I, the operation of induction motors under non-standard supply systems has been discussed in section II. The formulation of thermal model has been explained in section III. The simulation and experimental results are reported in section IV. And, finally the conclusions have been drawn in section V.

II. OPERATION OF INDUCTION MOTORS UNDER NON-STANDARD SUPPLY SYSTEMS

The most common forms of non-standard power supply are voltage unbalances between phases, distortion in supply system, voltage and frequency fluctuation. In many situations the motor may be connected direct-on-line, so any changes in the power supply will affect the motor operation. In order to predict the temperature profile under these situations a knowledge of motor dimensions as well as equivalent circuit parameters of the motors are very important. In this section the method of determination of equivalent circuit parameters are described. The equivalent circuit parameters are very useful to calculate the different losses take place in the motor.

The block diagram representation of the experimental set-up for conducting different test is shown in figure 1. The equivalent circuit parameters are obtained by conducting different tests as follows:

a. DC resistance measurement

The stator winding resistance of each phase of the motor, R_1 , is measured and temperature, T_1 °C, is noted. Since the resistance is a function of temperature, the resistance, R_2 , at any other temperature, T_2 , is calculated by (assuming copper conductor),

$$\frac{R_2}{R_1} = \frac{234.5 + T_2}{234.5 + T_1} \quad (1)$$

The power loss corresponding to the resistance R_2 should be taken into account for accurate temperature determination. If the resistances of different phases are different, the different losses need to be calculated and to be allocated in the model.

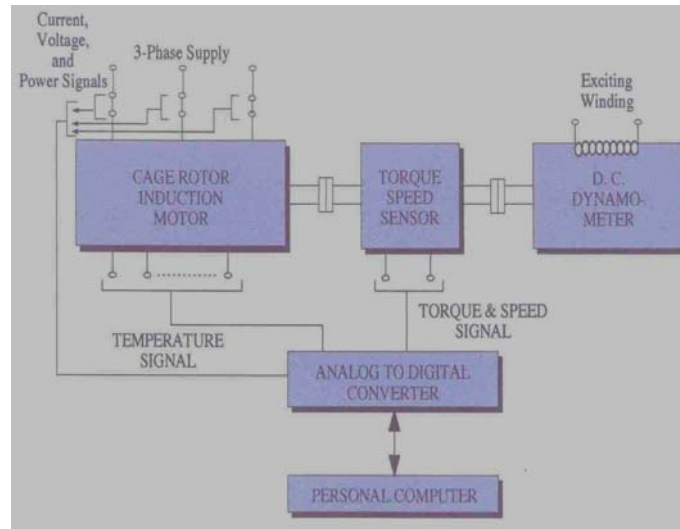


Figure 1: Block diagram representation of experimental set-up

b. Blocked rotor test at rated frequency

The equivalent circuit under blocked rotor operation is shown in figure 2. The slip, s , under blocked rotor condition is unity. R_1 and L_1 are the stator resistance and stator leakage inductance respectively. R_2 and L_2 are the rotor resistance and rotor leakage inductance referred to stator respectively. By measuring the voltage, current and power under this operation, total resistance and reactance are calculated. As the stator resistance R_1 is known from dc resistance measurement, the referred rotor resistance is calculated. The leakage inductances are divided equally. It is recommended to conduct the blocked rotor test at steady state temperature corresponding to normal motor operation.

c. Blocked rotor test at reduced frequency

For predicting the performance close to the actual one, the blocked rotor test should be conducted at or near the frequency of the rotor same as those existing in the operating conditions. Under normal operation the effective frequency in the rotor circuit is equal to slip frequency which is considerably low. So the blocked rotor test should be conducted at low supply frequency and the equivalent circuit parameters should be obtained at that frequency.

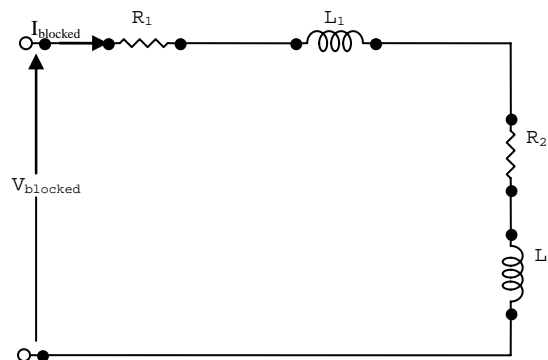


Figure 2: The equivalent circuit under blocked rotor operation

d. No load test at rated frequency

After allowing the motor to run for sufficient time at no-load, measurement of voltage, current, power and speed are taken at different voltages maintaining the frequency at the designed value. The equivalent circuit under no-load operation is shown in figure 3. The rotor circuit parameters are neglected.

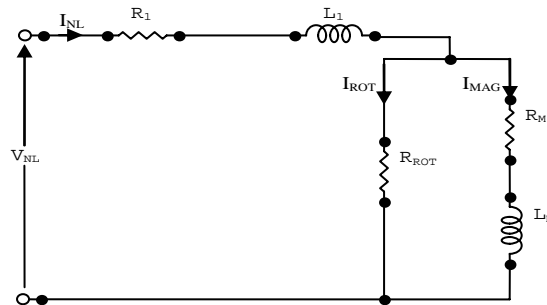


Figure 3: The equivalent circuit under no-load operation

The voltage, current and power input are measured under no-load operation and the equivalent circuit parameters, R_{ROT} , the resistance representing the rotational loss, R_M , the resistance representing the core loss, L_M , the inductance representing the magnetizing current are calculated.

e. Synchronism test

Since the rotor circuit parameters are neglected in the above test, there are some errors in the calculation of R_M and L_M . By running the rotor of the induction motor with the help of the DC dynamometer at a speed very close to the synchronous speed, the voltage, current, input power, frequency and speed are measured. The voltage supplied to the stator of the induction motor should be low. With proper calculation the parameters R_M and L_m can be calculated.

f. Reverse running test

Under unbalanced voltage operation the sequence components are used for calculation of motor currents and losses. The equivalent circuits corresponding to positive sequence and negative sequence are shown in figures 4a and b respectively. The parameters for the positive sequence are obtained in the normal method as described before. The reverse running test is conducted to obtain the parameters corresponding to the negative sequence. The rotor of the induction motor is driven by a dynamometer at normal operating speeds and balanced voltages of reduced magnitude but of negative sequence are applied to the stator winding. Measurements of line current, voltage, power and speed are taken for the calculation of the parameters.

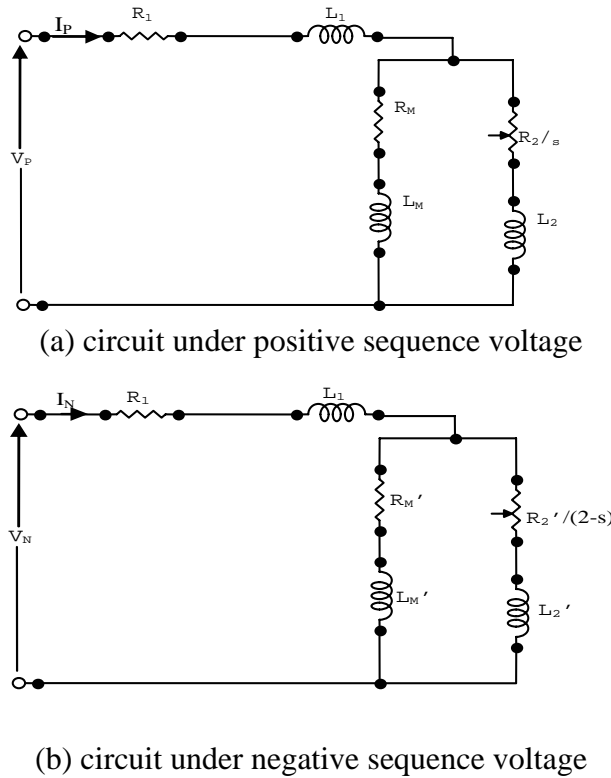


Figure 4: The equivalent circuit under unbalanced operation

g. Harmonic equivalent circuit parameters

The equivalent circuit for the k th harmonic is shown in figure 5a. At fundamental frequency, the slip is given by

$$s = \frac{\omega - \omega_r}{\omega} \tag{2}$$

where ω is the synchronous frequency in rad/s, and ω_r is the rotor speed in rad/s.

The slip for the k th harmonic is given by

$$s_k = \frac{k\omega - \omega_r}{k\omega} = 1 - \frac{1-s}{k} \tag{3}$$

Under normal operation, $s \ll 1$, so the slip $s_k, s_k = 1 \pm \frac{1}{k}$.

The current through the magnetizing part is negligibly small and can be neglected. So the approximate equivalent circuit can be represented as shown in figure 5b. From the measurement of voltage, current and power the parameters are calculated.

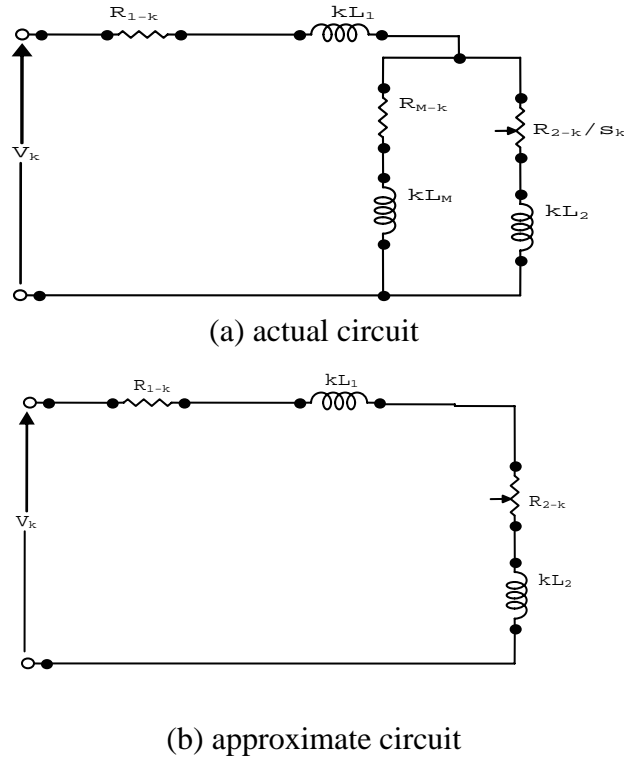


Figure 5: The equivalent circuit under harmonic condition

The determination of all above parameters is very important for accurate prediction of temperature. Other than the above equivalent circuit parameters the motor dimension and specification details are required to develop the thermal model.

III. FORMULATION OF HYBRID THERMAL MODEL

The hybrid thermal model used in this study for the determination of thermal condition along the cross-section of the motor is shown in figure 6. The nodes are distributed throughout the motor cross-section while the thermal capacitances are considered to be lumped at each node and thermal resistances between two consecutive nodes. There are multiple sources of heat within the motor: iron loss in the stator core and teeth, copper loss in stator winding, I^2R loss in rotor winding, tooth flux pulsation loss, windage loss, bearing friction loss etc. Some of these losses are non-linear function either of voltage, or speed and also depends on waveforms of supply system. Those losses are to be calculated from the operating condition. Associated with each source is a heat conduction path (combination of conduction, convection and/or radiation) to the environment.

The heat transfer equation is governed by usual Fourier's equation

$$\nabla \cdot K \nabla T + q = \rho C \left(\frac{\partial T}{\partial t} + u \cdot \nabla T \right) \quad (4)$$

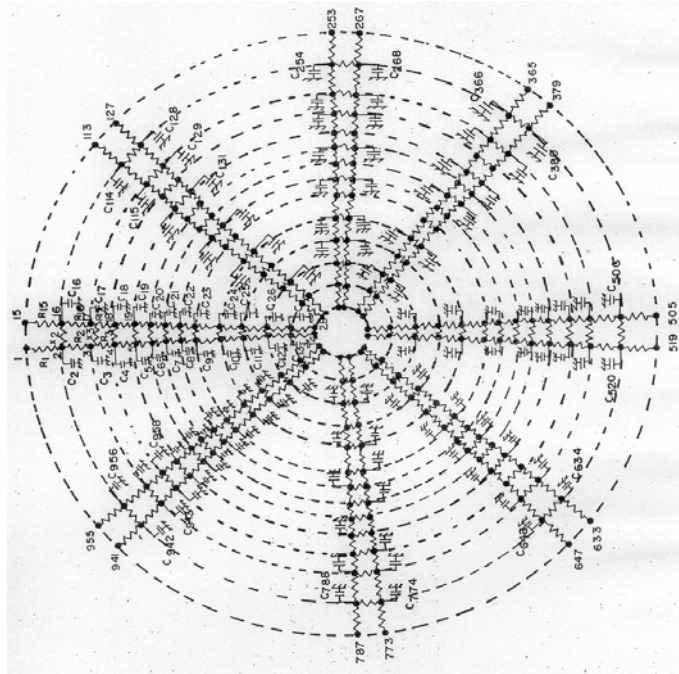


Figure 6: Hybrid thermal model of induction motor under transient condition

where T is the temperature, t is time, K is the thermal conductivity, q is the heat source (i.e., the internal generated heat per unit volume), u is the velocity, ρ is the density, C is the specific heat. While the equation (4) is expanded for two-dimension the heat equation under non-steady state condition is given by

$$K_x \frac{\partial^2 T}{\partial x^2} + K_y \frac{\partial^2 T}{\partial y^2} + q = \rho C \left(\frac{\partial T}{\partial t} + u_x \frac{\partial T}{\partial x} + u_y \frac{\partial T}{\partial y} \right) \quad (5)$$

where K_x and K_y are the thermal conductivities along the X and Y-axis respectively, u_x and u_y are the velocities along X and Y-axis respectively. A Cartesian coordinate system has been used in the model.

The equation (5) can be expanded and the equation for the central node, O, in terms of adjacent nodes a, b, c and d as shown in figure 7, can be expressed as

$$\frac{T_A - T_O}{R_{OA}} + \frac{T_B - T_O}{R_{OB}} + \frac{T_C - T_O}{R_{OC}} + \frac{T_D - T_O}{R_{OD}} + q_o = C_o \left(\frac{T'_O - T_O}{\partial t} + u_x \frac{T_C - T_A}{2\Delta x} + u_y \frac{T_D - T_B}{2\Delta y} \right) \quad (6)$$

where, T_O and T'_O represent the current and future temperature of the central node O respectively, q_o is the rate of heat generated at node O and is given by

$$q_o = q \Delta x \Delta y \Delta z \quad (7)$$

where Δx , Δy and Δz are the distances between two consecutive nodes along X, Y and Z-axis respectively. The Z-axis has been normalised as unity.

In equation (6), R_{OA} , R_{OB} , R_{OC} and R_{OD} represent the thermal resistances and are calculated by

$$R_{ij} = \frac{1}{K_{ij}} \frac{L_{ij}}{S_{ij}} \quad (8)$$

where K_{ij} is the thermal conductivity along the axis nodes i and j lie, L_{ij} is the distance between node i and j and S_{ij} is the area normal to heat flow path.

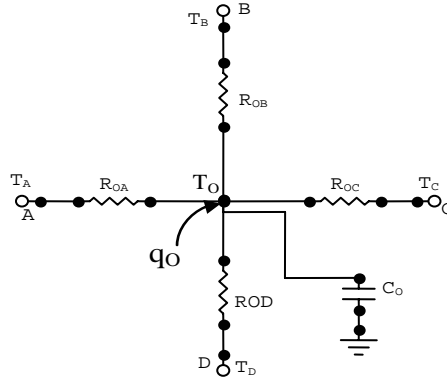


Figure 7: Representation of nodal network for 2-D heat flow

The thermal capacitance C_o associated with node O is given by

$$C_o = \rho C \Delta x \Delta y \Delta z \quad (9)$$

The material properties are shown in Table 1.

Table 1: Material properties

Material properties	Values	
Thermal conductivity (W/m K)	Iron	73
	Air	0.0241
	Copper	396
	Aluminium	202
	Insulation	0.05
Specific heat (J/kg K)	Copper	386
	Aluminium	900
Density (kg/m ³)	Copper	8900
	Aluminium	2700
	Iron	7800

The electrical conductivities of aluminium and copper are given as $2.9 * 10^7$ S/m and $5.4 * 10^7$ S/m respectively. The nonlinear temperature dependent electrical conductivity σ could be approximated as

$$\sigma = \frac{\sigma_0}{1 + \alpha(\Delta T)} \quad (10)$$

The electrical resistivity coefficient for aluminium and copper are given as $3.3 * 10^{-3} \text{ }^\circ\text{C}^{-1}$ and $3.93 * 10^{-3} \text{ }^\circ\text{C}^{-1}$ respectively.

The equation (8) is used to calculate the thermal resistances of different sections of the motor: frame, stator core, stator teeth, stator slot to stator core, stator slot to stator teeth, rotor slot to rotor teeth, rotor slot to rotor core, rotor teeth, rotor core and shaft. The thermal resistances between (i) frame and ambient, (ii) contact resistance between frame to stator laminations and (iii) air gap between stator and rotor are calculated separately.

The thermal resistance between frame and ambient such as R_f , R_{f5} , etc, (refer to figure 6) are calculated by

$$R_{frame} = \frac{\Delta T}{P_{node}} \quad (11)$$

where ΔT is the rise of frame temperature over ambient under full-load condition which is usually available from manufacturer and P_{node} is the power dissipated in each node.

The contact between stator lamination and frame is not perfect. Due to imperfect contact there is a need of introducing a thermal resistance and is calculated by

$$R_{f-s} = \frac{r_c}{S_c} \quad (12)$$

where r_c is the thermal contact resistance and depends on the metal involved, the surface roughness, the contact pressure, the materials occupying void spaces and temperature. S_c is the surface area around the node under consideration. The value of r_c has been chosen as $0.0006 \text{ m}^2 \text{ }^\circ\text{C}/\text{W}$ in the developed model.

The thermal resistance of air gap between stator and rotor, R_{ag} , is defined in terms of a dimensionless Nusselt number, N_{Nu} , the air gap length, l_g and is given by

$$R_{ag} = \frac{l_g}{N_{Nu} K_{air} S_{ag}} \quad (13)$$

The Nusselt number to be properly chosen as it depends on type of air flow, whether laminar or turbulent and cooling of the motor.

For accurate model the heat input must be calculated and allocated properly. The iron losses are calculated by

$$p = afB_p^2 + b(t_{lam} f B_p)^2 \quad (14)$$

where p is the power loss per kilogram, f is the frequency, t_{lam} is the thickness of lamination in millimeter, B_p is the peak value of flux density. Two constants a and b depends on motor dimension and are to be taken properly.

In motors with slots at both on stator and rotor, the flux density in the teeth varies as the relative position of the teeth varies. The amplitude of flux fluctuation in the stator teeth is given by

$$B_{p1} = \frac{\tau_{s2}}{2\tau_{s1}} \frac{K_{c2} - 1}{K_{c2}} B_{tm1} \quad (15)$$

where τ_{s1} and τ_{s2} are the slot pitches of stator and rotor respectively. K_{c2} is the Carter factor of the rotor and B_{tm1} is the maximum value of flux density in the middle of the tooth.

The pulsation loss in watts per kilogram of the teeth is given by

$$P_p = b(t_{lam} f_1 B_p)^2 \quad (16)$$

where the frequency f_1 is given by

$$f_1 = \frac{Q_2 * RPM}{60} \quad (17)$$

where Q_2 is the number of slots in the rotor and RPM is the speed of the motor.

The rotational loss due to friction of the bearing and wind is given by

$$P_{rot} = 5.4 * 10^5 (RPM)^{0.7} * P_{rated} \quad (18)$$

where P_{rated} is the rated power of the motor in watts.

It is seen that most of the parameters are non-linear functions of voltage, speed etc. The parameters are to be calculated properly and losses are to be determined correctly to allocate them to the concerned nodes. The final equation obtained around each and every node is a nonlinear equation which is to be solved for the determination of thermal condition around the cross-section of the motor.

IV. Simulation and experimental results

The model has been applied to a small 5 kW 4 pole motor. The specification of the motor are: Three phase cage-rotor induction motor, 5 kW, 415 V, 9 A, 50 Hz, 1435 RPM. The other details are: Class of insulation is B, stator slots 36, rotor slots 44, stator outer diameter 270 mm, rotor outer diameter 155 mm, core length 140 mm, stator resistance per phase 4.8 Ω and rotor resistance referred to stator is 4.5 Ω . The operating supply system of the motor are analysed and the sequence component of voltages and harmonic component of voltages are calculated. From test and manufacturer's specification all equivalent circuit parameters are obtained. The experimental set-up is shown in figure 8.



Figure 8: The experimental set-up of motor and dynamometer

After calculating all the thermal resistances and capacitances and allocating the losses to each node, the temperature of each node is obtained by rearranging the equation (6)

$$T_{O(i,j)}^{\dot{}} = T_{O(i,j)} + \Delta t * \left(\frac{T_{i-1,j} - T_{i,j}}{R_{i-1,j} C_{i,j}} + \frac{T_{i+1,j} - T_{i,j}}{R_{i+1,j} C_{i,j}} + \frac{T_{i,j-1} - T_{i,j}}{R_{i,j-1} C_{i,j}} + \frac{T_{i,j+1} - T_{i,j}}{R_{i,j+1} C_{i,j}} + \frac{q_{O(i,j)}}{C_{O(i,j)}} - u_x \frac{T_{i+1} - T_{i-1}}{2\Delta x C_{O(i,j)}} - u_y \frac{T_{j+1} - T_{j-1}}{2\Delta y C_{O(i,j)}} \right) \quad (19)$$

The starting values of all nodes are taken to be equal to the ambient temperature. The time step Δt should be carefully selected and is to be less than the minimum value of associated thermal time constant of all nodes.

The motor was run for sufficient time to allow temperature to attain steady state and with different output condition. The figure 9 shows the variation of temperature rise as a function of power output. The surface temperature is measured by a thermometer while the winding temperature is calculated from the difference of winding resistance. The error between the simulated and experimental results is within $\pm 2^\circ\text{C}$. The actual temperature of surface is slightly less than the predicted values due to the effect of air flow at outside.

The motor was run under no-load condition for half-an-hour and then loaded to full-load and run for an hour. The surface temperature was measured by a thermometer. The figure 10 shows the comparison of the transient temperature rise of the surface obtained from the model and experiment respectively. The predicted temperature rise is very close to the experimental values.

The unbalancing has been introduced in the supply system by adjusting the phase voltages. The negative sequence voltage is calculated. With the constant magnitude of negative sequence voltage the motor is allowed to run continuously to attain the steady state temperature at no-load. Since the currents in the three phases are different from each other, the losses and consequently the temperature rise of the winding will also be different. The figure 11 shows the predicted and

measured temperature rise of the three windings as a function of negative sequence voltage under no-load condition.

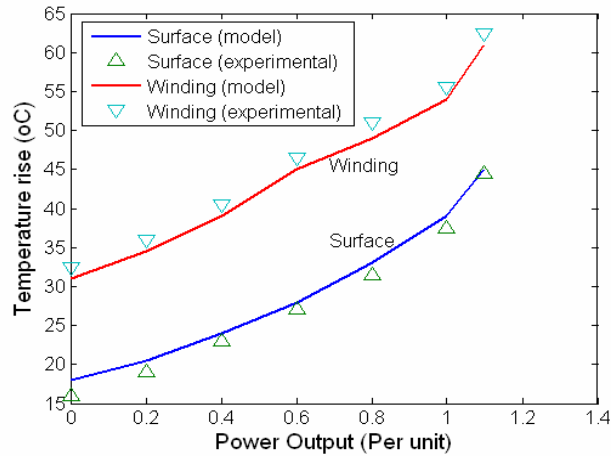


Figure 9: The temperature rise as a function of power output

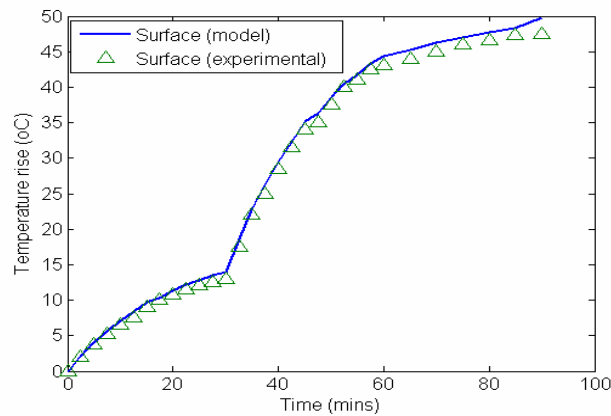


Figure 10: Surface temperature under transient condition; No-load for 30 minutes, and then full-load for 1 hour

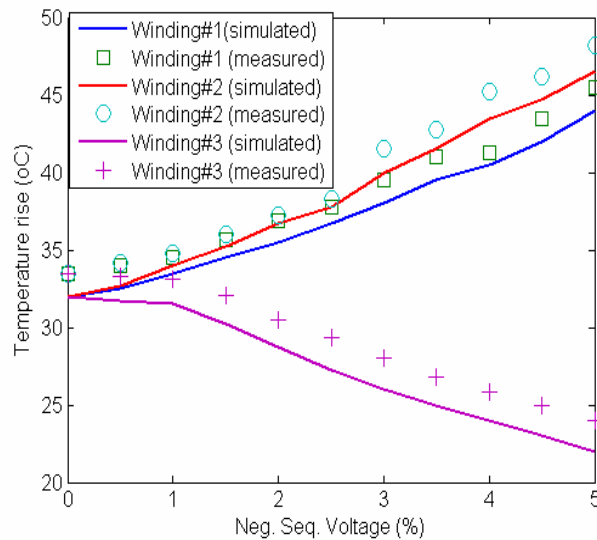


Figure 11: The temperature rise of three windings as a function of negative sequence voltage

To verify the developed model under harmonic voltage condition, the harmonics have been introduced in the supply system. The figure 12 shows the variation of the winding as well as surface temperature rise as a function of harmonic voltage at no-load condition. It is seen that the severity of the effect of harmonics on the temperature rise is less compared to negative sequence voltage. The predicted as well as measured temperature rises of all the windings are very similar.

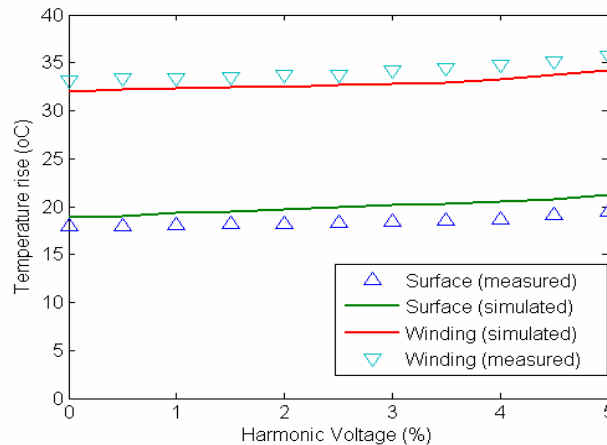


Figure 12: Temperature rises of winding and surface as a function of harmonic content

The developed model can be very useful in many different abnormal operating conditions. One of such condition which is very common in many countries is the variation of ambient temperature. Since it may not be possible to have controlled temperature condition for all motors to operate, this model can be used to determine how much the output should be derated with the increase in ambient temperature. Usually the designer assumes the ambient temperature as 20°C and the motor is designed for 10% continuous overload. The maximum temperature rise of the winding is kept constant to determine the derating. The figure 13 shows the variation of available per unit output as a function of ambient temperature. It is seen that the motors need to be derated if the ambient temperature increases considerably. The model can be very useful in many other abnormal situations.

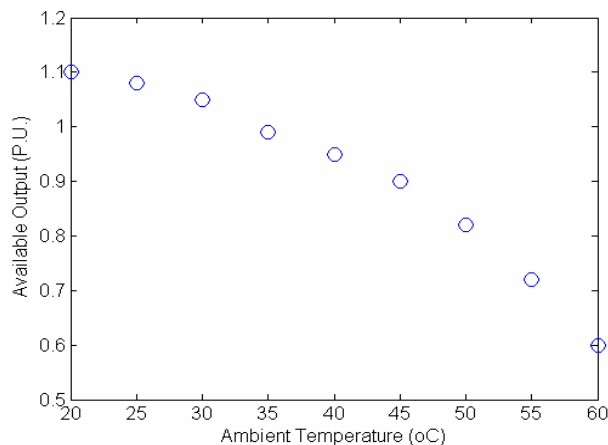


Figure 13: Predicted available output as a function of ambient temperature

V. Conclusions

This paper has described the development of a hybrid thermal model for accurate estimation of thermal condition of cage-rotor induction motors under non-standard supply systems. The developed thermal model is a combination of lumped and distributed thermal parameters which are available from motor dimensions and other physical constants. The equivalent circuit parameters of the motors under different operating conditions are obtained experimentally. The thermal condition of the motor under non-standard supply systems such as unbalanced power supply, distorted power supply can be estimated and the necessary derating of the motor can be carried out. The predicted temperature is very close to the experimental values. The model can be very useful to determine the thermal condition of the motor in many stringent operating conditions.

REFEREMCES

- [1] J. Driesen, R. Belmans, K. Hameyer, "Coupled thermo-magnetic simulation of a foil-winding transformer connected to a non-linear load", IEEE transactions on Magnetics, Vol. 36, No. 4, pp. 1381-1385, July 2000.
- [2] D. Staton, A. Boglietti and A. Cavagnino, "Solving the more difficult aspects of electric motor thermal analysis in small and medium size industrial induction motors", IEEE transactions on Energy Conversion, Vol. 20, No. 3, pp. 620-628, Sep. 2005.
- [3] M.N. Sabry, "High-precision compact thermal models", IEEE transactions on Components and Packaging Technologies, Vol. 28, No. 4, pp. 623-629, Dec. 2005.
- [4] W.D.Walker and W.F.Weldon, "Thermal modelling and experimentation to determine maximum power capability of SCR's and thyristors", IEEE transactions on Power Electronics, Vol. 14, No. 2, pp. 316-322, Mar. 1999.
- [5] L. I. Zhu, X.. J. Zheng, "A theory for electromagnetic heat conduction and a numerical model based on Boltzmann equation", International Journal of Nonlinear Sciences and Numerical Simulation, Vol. 7 No. 3, pp. 339-344, 2006.
- [6] S.C. Mukhopadhyay and S.K. Pal, "Temperature analysis of induction motors using a hybrid thermal model with distributed heat sources", Journal of Applied Physics, Vol. 83, No. 11, pp. 6368-6370, June 1998.
- [7] P.K. Vong and D. Rodger, "Coupled electromagnetic-thermal modelling of electrical machines", IEEE transactions on Magnetics, Vol. 39, No. 3, pp. 1614-1617, May 2003.
- [8] Y.G. Guo, J. G. Zhu and W. Wu, "Thermal analysis of soft magnetic composite motors using a hybrid model with distributed heat sources", IEEE transactions on Magnetics, Vol. 41, No. 6, pp. 2124-2128, June 2005.

[9] S. Mezani, N. Takorabet and B Laporte, "A combined electromagnetic and thermal analysis of induction motors", IEEE transactions on Magnetics, Vol. 41, No. 5, pp. 1572-1575, May 2005.

[10] M.I.L. Jamal, J. Fouladgar, E. H. Zaim and D. Trichet, "A magneto-thermal study of a high-speed synchronous reluctance machine", IEEE transactions on Magnetics, Vol. 42, No. 4, pp. 1271-1274, April 2006.

[11] M. J. Duran and J. Fernandez, "Lumped-parameter thermal model for induction machines", IEEE transactions on Energy Conversion, Vol. 19, No. 4, pp. 791-792, Dec. 2004.

[12] A.L. Shenkman and M. Chertkov, "Experimental method for synthesis of generalized thermal circuit of polyphase induction motors", IEEE transactions on Energy Conversion, Vol. 15, No. 3, pp. 264-268, Sep. 2000.

[13] M. Dehghan, "Implicit collocation technique for heat equation with non-classic initial condition", International Journal of Nonlinear Sciences and Numerical Simulation, Vol. 7 No. 4, pp. 461-466, 2006.

[14] R. Zhang, C. Zhang, J. Jiang, "A new approach to direct solution of 2D heat transfer problem with non-linear source terms in frequency domain", International Journal of Nonlinear Sciences and Numerical Simulation, Vol. 7 No. 3, pp. 295-298, 2006.

[15] X.Z. Bai, Y.M. Fu, H.H. Zhang, "Advances in research on electromagnetic heating effects to stop crack propagation in metal components", International Journal of Nonlinear Sciences and Numerical Simulation, Vol. 4, No. 1, pp. 47-58, 2003.

[16] X.Z. Bai, Y.M. Fu, Y.D. Hu, L.J. Zheng, "Temperature field around crack tip in a current-carrying plate under the repeated action of pulse current", International Journal of Nonlinear Sciences and Numerical Simulation, Vol. 4 No. 1, pp. 59-66, 2003.

[17] C.C. Hwang, S.S. Wu and Y. H. Jiang, "Novel approach to the solution of temperature distribution on the stator of an induction motor", IEEE transactions on Energy Conversion, Vol. 15, No. 4, pp. 401-406, Dec. 2000.